processes

MDPI

Article

Extra-Heavy Crude Oil Viscosity Reduction Using and Reusing Magnetic Copper Ferrite Nanospheres

Lucía Mateus [1,†], Esteban A. Taborda [2,†], Carlos Moreno-Castilla [3], María Victoria López-Ramón [4,*], Camilo A. Franco [5] and Farid B. Cortés [5,*]

1 Facultad de Ciencias, Universidad de Ciencias Aplicadas y Ambientales U.D.C.A., Bogotá 111166, Colombia; olga.mateus@udca.edu.co
2 Vicepresidencia de Exploración, ECOPETROL, Bogotá 110321, Colombia; esteban.taborda@ecopetrol.com.co
3 Departamento de Química Inorgánica, Universidad de Granada, 18071 Granada, Spain; cmoreno@ugr.es
4 Departamento de Química Inorgánica y Orgánica, Universidad de Jaén, 23071 Jaén, Spain
5 Grupo de Investigación en Fenómenos de Superficie—Michael Polanyi, Departamento de Procesos y Energía, Facultad de Minas, Universidad Nacional de Colombia, Sede Medellín, Medellín 050034, Colombia; caafrancoar@unal.edu.co
* Correspondence: mvlro@ujaen.es (M.V.L.-R.); fbcortes@unal.edu.co (F.B.C.)
† These two authors contributed in equal proportions.

Abstract: The main objective of this study is the synthesis, use, and reuse of magnetic copper ferrite nanospheres (CFNS) for extra-heavy oil viscosity reduction. The CFNS were synthesized using a solvothermal method resulting in mean particle size of 150 nm. Interactions of CFNS with the crude oil were evaluated through asphaltene adsorption isotherms, as well as static and dynamic rheology measurements for two cycles at 25 °C. Adsorption and desorption experiments corroborated that most of the asphaltenes adsorbed can be removed for nanoparticle reuse. During the rheology tests, nanoparticles were evaluated in the first cycle at different concentrations from 300 to 1500 mg/L, leading to the highest degree of viscosity reduction of 18% at 500 mg/L. SiO_2 nanoparticles were evaluated for comparison issues, obtaining similar results regarding the viscosity reduction. After measurements, the CFNS were removed with a magnet, washed with toluene, and further dried for the second cycle of viscosity reduction. Rheology tests were performed for a second time at a fixed concentration of 500 mg/L, and slight differences were observed regarding the first cycle. Finally, changes in the extra-heavy oil microstructure upon CFNS addition were observed according to the significant decrease in elastic and viscous moduli.

Keywords: magnetic copper ferrite nanospheres; extra-heavy crude oil; viscosity reduction; nanomaterial reuse

Citation: Mateus, L.; Taborda, E.A.; Moreno-Castilla, C.; López-Ramón, M.V.; Franco, C.A.; Cortés, F.B. Extra-Heavy Crude Oil Viscosity Reduction Using and Reusing Magnetic Copper Ferrite Nanospheres. *Processes* **2021**, *9*, 175. https://doi.org/10.3390/pr9010175

Received: 3 December 2020
Accepted: 15 January 2021
Published: 19 January 2021

1. Introduction

The current petroleum reserves worldwide are mainly attributed to heavy (HO) and extra-heavy (EHO) crude oils, which represent the double regarding for the conventional oils [1,2]. In particular, Colombia is not distant from the worldwide panorama, where EHO and HO represent around 60% of the total production [3,4]. However, different processes in the oil and gas (O&G) industry remain challenging due to these crude oils' complexity, including the production, transport, and refining. Crude oils have a low API gravity and high viscosity generally attributed to the high content of asphaltenes and resins and the possible viscoelastic network between these compounds [5–12]. Various fluids such as light crude oil, naphtha, diesel, and others, as well as gases (mainly CO_2), are commonly used to reduce the viscosity of crude oils [13–16]. However, these solvents can generate asphaltenes' instability, further blocking the formation and oil pipelines [13,14]. In Colombia, for example, between 2005 and 2016 the crude oil transport increased from 150,000 to 450,000 bpd, with naphtha the solvent most often used for diluting HO and EHO to reach conditions for pipeline transport (400 cSt @ 311 K, 18° API, and BSW < 0.5%) [17–21].

Improving HO and EHO mobility by reducing viscosity has been a topic of significant interest [19,22–32]. For instance, the company Geo Estratos S.A. [33] reported using different viscosity-reducing agents based on terpolymers, with up to 60% viscosity reduction with a dosage of 3% v/v. Mortazavi-Manesh and Shaw [34] evaluated the rheological properties of Maya crude oil using different solvents at different temperatures, showing that the toluene + butanone mixture was the best of the mixes evaluated. Gateau et al. [25] also studied the blend between solvents and naphtha for reducing oil viscosity reduction. However, a high amount of solvents is required, which can generate asphaltene precipitation and create environmental hazards from the generation of polluting gases [35]. Oil-in-water (O/W) emulsions are also an alternative for improving the transport of HO and EHO [22,31]. This process has been used at the industrial level in Venezuela and labeled Orimulsion® [19,36–38].

Moreover, a few authors have recently evaluated the use of nanoparticles and nanofluids for HO viscosity reduction [39–42]. In our previous studies [43–46], nanoparticles of different chemical natures (SiO_2, Al_2O_3, Fe_2O_3, etc.) have been synthesized for dispersion into fluids. The main mechanism of viscosity reduction upon nanoparticles' addition is the modification of the heavy crude oil's internal structure [44]. However, the nanoparticles' reuse has not been evaluated due to removing the nanomaterial from oil is a complicated task and could increase the costs of the transporting process. The nanomaterial separation process also depends on the efficiency and the nanofluid dosage, which generates an economically unviable situation.

Consequently, this study proposes a novel solution by evaluating nanoparticles with magnetic characteristics capable of being removed from the fluid and reused in new viscosity reduction cycles. In this method, the additional cost of adding the particles will be reduced due to the reuse of the nanoparticles. The procedure aims to enhance the production and transportation processes, reducing the problems associated with these processes previously mentioned. Therefore, this work's main objective is to evaluate the use and reuse of copper ferrite nanospheres (CFNS) to reduce the viscosity of EHO. The process takes advantage of the magnetic properties of CFNS, which allows them to be easily removed from the crude oil matrix using a magnet once the first cycle of viscosity reduction has finished. In this manner, different dosages of nanoparticles were added to the crude to reduce viscosity. Additionally, two viscosity-reduction cycles were evaluated, removing the nanoparticles from the oil, washing them, and adding them again, with similar performances to the first cycle of viscosity reduction. The results of this study suggest that the use of this class of particles is capable of enhancing heavy crude transport and mobility processes and offers a complementary technique to conventional processes with promising performances for the O&G industry.

2. Materials and Methods

2.1. Materials

Sodium acetate, ethylene glycol, polyethylene glycol, $CuCl_2{\cdot}2H_2O$ and $FeCl_3{\cdot}6H_2O$ of high purity were used as reagents for the synthesis of copper ferrite nanospheres. n-Heptane was used for asphaltene isolation from an extra heavy crude oil (EHO). Toluene (99.8%) was used in the asphaltene adsorption test. All chemical reagents used were of high purity and supplied by Sigma-Aldrich (Madrid, Spain).

2.2. Synthesis of Copper Ferrite Nanospheres

CFNS was prepared by a solvothermal method described elsewhere [47]. For this purpose, $CuCl_2{\cdot}2H_2O$ and $FeCl_3{\cdot}6H_2O$ were dissolved in ethylene glycol to form a clear solution, followed by the addition of sodium acetate and polyethylene glycol. The mixture was vigorously stirred for 30 min and then sealed in a 125-mL Teflon-lined stainless-steel autoclave, which was heated to 200 °C for 12 h before cooling to room temperature. The black solid was centrifuged and washed three times with ethanol (50 mL/g) and dried at 60 °C for 8 h.

2.3. Physicochemical Characterization Methods

The morphology of CFNS was assessed with a transmission electron microscope (TEM) and a scanning electron microscope (SEM). TEM experiments were carried out with a JEOL JEM-1010 microscope (JEOL Europe SAS, Croissy, France), and SEM micrographs were obtained with Carl Zeiss SMT equipment (Carl Zeiss SMT, Oberkochen, Germany). The Brunauer–Emmett–Teller surface area (S_{BET}) was determined fromN_2 adsorption–desorption isotherm at –196 °C, obtained with an Autosorb 1 from Quantachrome (Boynton Beach, FL, USA). X-ray photoelectron spectroscopy (XPS) was performed using an EscaLab 200R system (Thermo Fisher Scientific, East Grinstead, UK) equipped with an MgKα X-ray source and a hemispherical electron analyzer [47].

The crystalline structure of CFNS was characterized by X-ray diffraction (XRD) and collected on an X-ray Empyrean diffractometer with a PIXcel3D detector (Malvern Panalytical, Almelo, The Netherlands) under the following experimental conditions: CuKα radiation, 40 kV and 30 mA, in a 2θ range between 10 and 70° with 0.01° step size and an integration time of 100 s. Identification and quantification of the different phases present in each sample were assessed using a Rietveld refinement method [48,49] using HighScore Plus software [50] and the Crystallography Open Database [51].

A Superconducting Quantum Interface Device (SQUID) magnetometer (Quantum Design model MPMS-XL, San Diego, CA, USA) was used to record the magnetization (M) of CFNS at room temperature as a function of the magnetic field applied (H). The magnetic hysteresis (M-H) curve describes the magnetic response of the material and permits measurement of the saturation (M_S), remnant magnetization (M_R), and coercivity (H_C).

2.4. Extra-Heavy Crude Oil

The EHO sample has a 20% content of asphaltene, as well as an API gravity of 6.4° at 15.6 °C. n-C_7 asphaltenes were obtained as described elsewhere [52–54]. The elemental analysis showed a content of 81.7, 7.8, 0.3, 6.6, and 3.6% wt. of C, H, O, N, and S, respectively. In addition, n-C_7 asphaltene's molecular weight of 907.3 g/mol was obtained through vapor pressure osmometry.

2.5. Adsorption/Desorption Tests

The adsorption and desorption cycles were evaluated in this manuscript, as described below. n-C_7 asphaltenes were dissolved in toluene at different concentrations up to 3000 mg/L. A fixed amount of 100 mg of CFNS was added to 10 mL of solution and kept under 200 rpm for 24 h [53,55]. The amount adsorbed "N_{ads}" (mg/g) is obtained as follows:

$$N_{ads} = (C - C_E) * (V/W) \quad (1)$$

where C and C_E are the concentrations of the n-C_7 asphaltenes before and after adsorption onto de CFNS, W (g) is the dry mass of CFNS, and V (L) the solution volume. C_E is obtained through absorbance changes using a GENESYS 10S UV-vis spectrophotometer (Thermo Scientific, Waltham, MA, USA), as reported in previous studies [53,55–57]. This test was performed in triplicate.

CFNS with adsorbed n-C_7 asphaltenes were dried (120 °C and 24 h) before evaluating the desorption tests. Then, the dried material was added to pure toluene and stirred for 72 h at 200 rpm, and the remaining adsorbed n-C_7 asphaltenes "$N_{ads,rem}$" (mg/g) is calculated as follows [58,59]:

$$N_{ads,rem} = N_{ads} - C_{E,rem} * (V/W) \quad (2)$$

where $C_{E,rem}$ (mg/L) is the asphaltene concentration in toluene after the desorption process.

2.6. Rheological Measurements

2.6.1. Steady-State Rheology

The effect of CFNS on crude oil rheological properties was assessed through steady-state and dynamic rheological measurements, as reported in previous studies [44,45,60,61].

For this, a Kinexus Pro rotational rheometer (Malvern Instruments, Worcestershire, UK) was employed. The effect of the concentration was evaluated by adding CFNS to the EHO matrix at different concentrations (300, 500, 700, 1000, and 1500 mg/L). The rheological measurements were evaluated in a shear rate range 1–100 s^{-1} at 25 °C, which was done in triplicate. Nanoparticles were added to the crude oil matrix by stirring at 500 rpm for 30 min until homogenization [44]. To evaluate the reuse of the CFNS in the process of reducing the viscosity of EHO, we conducted a new measurement labeled as the second cycle of viscosity reduction by adding CFNS. The nanoparticles previously added to the EHO matrix were removed from the crude oil, taking advantage of their magnetic properties by adding a magnet and manually stirring the crude oil. Subsequently, the magnet with the nanoparticles adhered to the surface was manually removed. The CFNS nanoparticles were then removed and reconditioned for use by means of a rigorous 10 h wash with toluene. The first cycle step was repeated, but only 500 mg/L were added (the best dosage obtained from the first round of rheological tests).

2.6.2. Dynamic Rheology Measurements

Dynamic rheology (oscillometry tests) were conducted with amplitude and frequency sweep tests. A strain-sweep test was performed to evaluate the linear viscoelasticity region. In addition, an oscillatory amplitude test was made for viscoelastic moduli estimation of EHO and first- and second-cycle EHO with 500 mg/L CFNS nanoparticles were performed using a rotational rheometer Kinexus Pro (Malvern, UK). A fixed frequency (ω) of 10 rad/s was employed, and the percentage of strain (γ) varied between 0.1% and 100% at a. A strain value of 2% was employed for dynamic rheological tests [62–65]. Finally, a frequency range of 0.1–100 rad/s at 25 °C was used for oscillatory frequency tests.

3. Modeling

Solid–Liquid Equilibrium (SLE) Model

The solid–liquid equilibrium (SLE) model was employed to describe the adsorption of self-associative molecules such as asphaltene over the CFNS [66,67]. In addition, The Herschel–Bulkley (H-B) model was employed to describe the effect of CFNS in the rheological behavior of EHO [68,69]. The correlation coefficient (R^2) and root-mean-square error (RMSE) were used to estimate the suitability of fit using the Solver feature in Excel package 2015 [70–74]. Expressions both the SLE and H-B model are shown below, and related parameters are summarized in Table 1.

Table 1. Expressions and related parameters of the solid–liquid equilibrium (SLE) and Herschel–Bulkley (H-B) models.

Model	Parameters
SLE	N_{ads} (mg/g): amount adsorbed $N_{ads,m}$ (mg/g): maximum adsorption capacity C_E (mg/g) is the equilibrium concentration of n-C_7 asphaltenes. K (g/g): the degree of n-C_7 asphaltenes self-association over the CFNS surface H (mg/g): and Henry's law constant related to adsorption affinity
H-B	μ: viscosity at a determined shear rate γ (s^{-1}): shear rate n_H: index of flow behavior K_H (Pa s^n): consistency index $\mu_{0,\gamma}$ (cP): viscosity at zero stress $\mu_{\infty,\gamma}$ (cP): viscosity at infinite stress

For the solid–liquid equilibrium (SLE):

$$C_E = \frac{\psi H}{1 + K\psi} \exp\left(\frac{\psi}{N_{ads,m}}\right) \quad (3)$$

where,

$$\psi = \frac{-1 + \sqrt{1 + 4K\xi}}{2K};\ \xi = \left(\frac{N_{ads,m} \cdot N_{ads}}{N_{ads,m} - N_{ads}} \right)$$

And for H-B model:

$$\mu = K_H(\gamma^{(n_H - 1)}) + \mu_{\infty,\gamma} \quad (4)$$

4. Results and Discussion

Previous results indicate that SiO_2 nanoparticles (8 nm) can selectively adsorb asphaltenes and resins on their surface [53], leading to changes in the asphaltenes aggregates and further viscosity reduction. Hence, these particles are selected to compare the performance of CFNS on the viscosity change of the EHO. The results are divided into four parts: (1) the physicochemical characterization of the CFNS sample, (2) rheology studies at a steady state in the presence and absence of CFNS for the first and second use cycles, (3) dynamic oscillometry of HO in the presence and absence of CFNS for the first and second use cycles, and (4) the asphaltene adsorption isotherms on CFNS.

4.1. Characteristics of the CFNS Sample

Figure 1a,b depicts TEM and SEM images, respectively, showing that CFNS is composed of nanospheric particles with a mean diameter of 150 nm, which was determined by an open-source image processing program ImageJ based on different TEM images and an SBET value of 47 m^2/g. Figure 1c shows the XRD patterns of CFNS, which was composed of three phases: cubic $CuFe_2O_4$ (67.5%), Cu_2O (17.1%), and Cu (15.4%), with average crystallite sizes of 7.7, 9.8, and 90.0 nm, respectively. The presence of metallic Cu and Cu^+ ions was due to the reduction by ethylene glycol of some Cu^2+ ions present in the solution [75–80].

XPS was used to investigate the oxidation state and coordination number of the metal ions on the outermost surface of the CFNS sample. Figure 1d,e depicts the XPS profiles of Fe and Cu 2p core-level regions, respectively. Deconvolution of the broad Fe 2p3/2 peak showed two more peaks. The first peak occurred at a BE of 709.8 eV, which was accompanied by a satellite peak at a BE of around 718.5 eV, indicating the presence of Fe^{3+} cations [6]. The second peak occurred at 711.3 eV, between the first peak and its satellite, indicating the presence of Fe3+ cations in more than one coordination environment, that is, A sites at a higher BE (second peak) and B sites at a lower BE (first peak) [81]. The Cu 2p3/2 profile showed two peaks at 932.3 and 933.5 eV, assigned to reduce copper species (Cu^0/Cu^+) and Cu^{2+}, respectively, and a shake-up satellite at around 942 eV, indicating the presence of Cu^{2+} [82,83]. The Cu/Fe surface atomic ratio was 0.22, which was lower than the theoretical value of 0.5, indicating that Fe ions were segregated to the CFNS surface.

Figure 1f depicts the M-H curve of CFNS. The MS, MR, and HC values were 49.20 emu/g, 0.78 emu/g, and 15 Oe, respectively, with an MR/MS ratio of 0.02, indicating a superparamagnetic behavior of CFNS.

4.2. Asphaltene Adsorption/Desorption Experiments

The viscosity reduction is mainly driven by the interaction between the heavy components of the EHO (mainly, the aggregates of n-C_7 asphaltenes) and the CFNS. To understand this interaction, we have evaluated the adsorption equilibrium based on the adsorption isotherms. Figure 2 shows the adsorbed amount of n-C_7 asphaltenes regarding the equilibrium concentration when CFNS is added into the solution model. Figure 2 shows the adsorption (cycles 1 and 2) and desorption isotherms of n-C7 asphaltene on CFNS at 25 °C obtained from the batch mode, obtaining a deviation lower than 5%, considering both curves nearly equal. Adsorption isotherms are Type I according to the International Union of Pure and Applied Chemistry, where the adsorbed amount of n-C_7 asphaltenes rises as C_E increases until a plateau is reached. The obtained SLE parameters support this behavior; mainly, the maximum adsorbed uptake (Table 2). Iron has a high-affinity asphaltene adsorption according to the selectivity toward heteroatoms such as nitrogen in the forms of amine,

quaternary-N, pyridine, and pyrrolic [84]. Among these, due to its aromatic nature and the increase in the atomic ratio, pyridines could be the main source for interaction with CFNS due to both σ and π bonding [85,86]. Note that the adsorptive capacity of CFNS in cycle 1 is slightly higher than cycle 2, especially at low concentrations that also indicate higher adsorption affinity and is corroborated by the SLE model's estimated H parameter. This is confirmed by the values of the h parameter of the SLE model. These results agree with findings reported by Nassar et al. [55], Montoya et al. [66], and Arias-Madrid et al. [85].

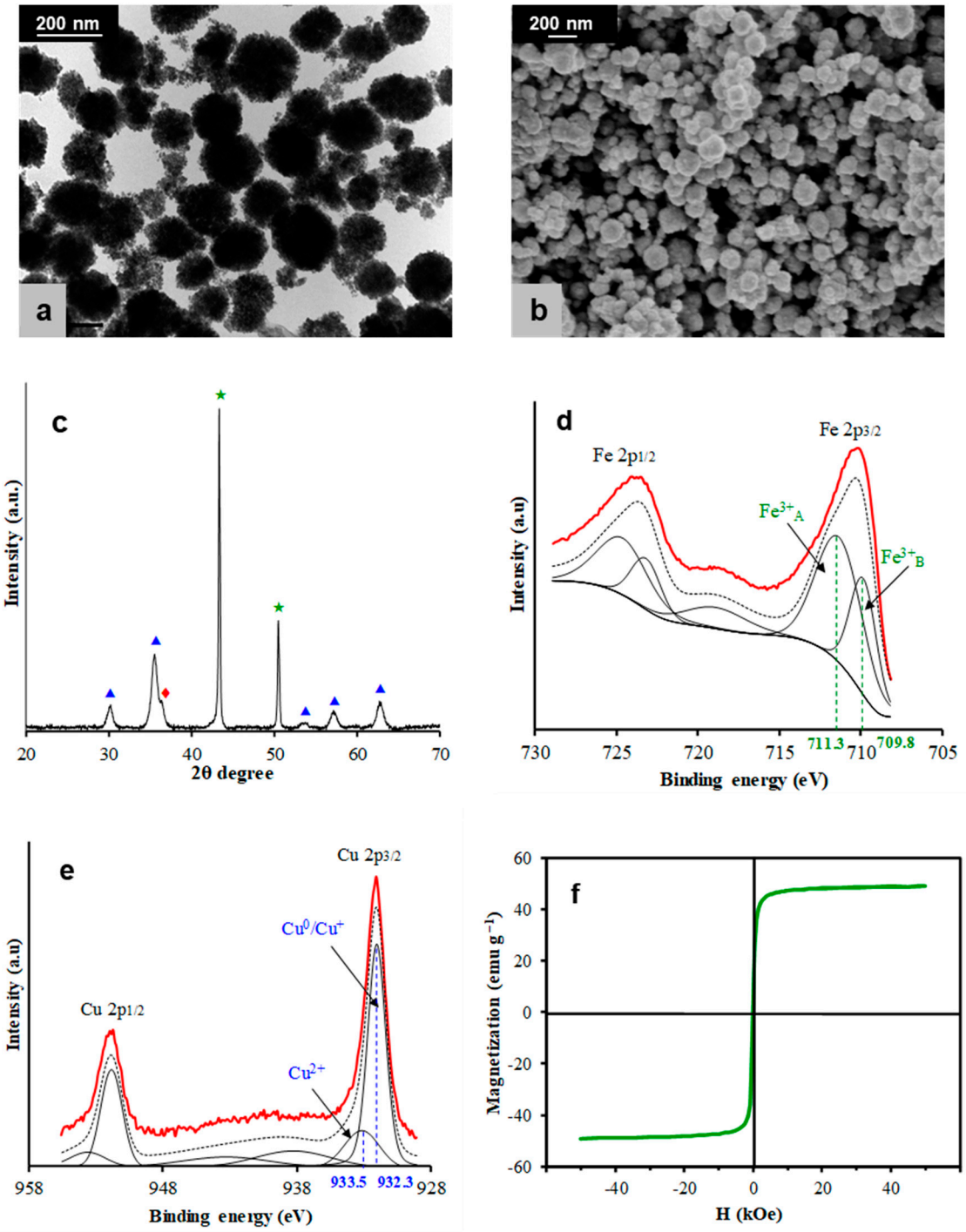

Figure 1. (**a**) TEM and (**b**) SEM micrographs of copper ferrite nanospheres (CFNS). (**c**) XRD patterns of the CFNS catalyst: (▲) cubic spinel; (★) copper; (◆) cuprite. (**d**) and (**e**) XPS profiles of the Fe2p and Cu2p regions, respectively, and (**f**) magnetization versus the applied magnetic field.

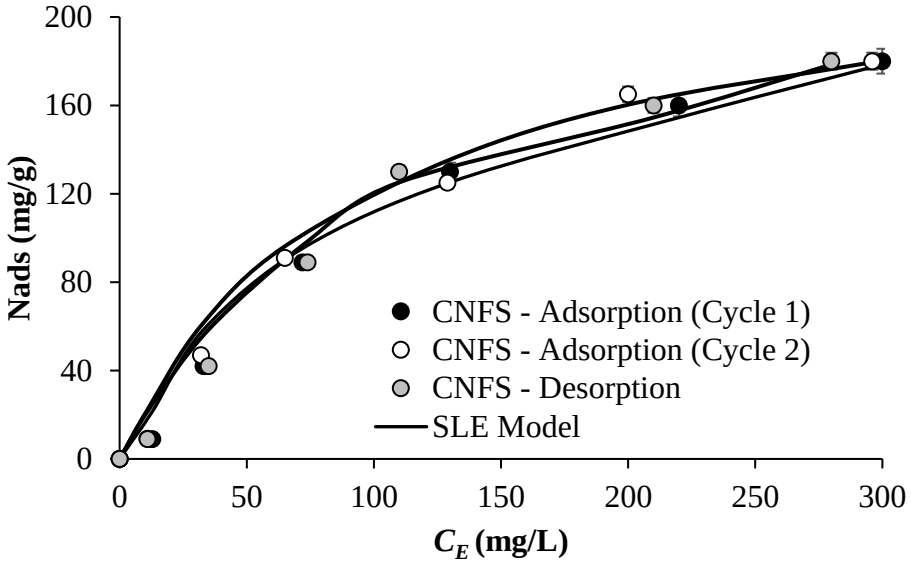

Figure 2. Asphaltene adsorption/desorption isotherm on CFNS, and SLE model correlation at 25 °C.

Table 2. Parameters estimated from the solid–liquid equilibrium (SLE) model for n-C_7 asphaltene adsorption/desorption on CFNS.

Sample	H (mg/g)	$K \times 10^{-4}$ (g/g)	$N_{ads,m}$ (mg/g)	R^2	RMSE
CFNS cycle 1	1.24	1.9	472.5	0.96	6.84
CFNS cycle 2	1.27	2.1	413.2	0.97	5.79
CFNS (desorption)	1.35	3.4	407.6	0.99	4.99

From Figure 2, it is possible to conclude that the adsorption and desorption process on CFNS at 25 °C is reversible. The loops of adsorption and desorption for the CFNS are similar, showing a clear case of reversibility in this process, which favors their reuse in the EHO reduction process. This opens the landscape for the use and reuse of these materials for applications to improve EHO mobility.

4.3. Steady-State Measurements of Heavy Crude Oil

4.3.1. First CFNS Cycle for Viscosity Evaluation

Figure 3 shows the rheological evaluation through the flow curve of the EHO and its mixtures with CFNS at different concentrations (300, 500, 700, 1000, and 1500 mg/L). The behavior described for the evaluated samples is typical of this class of fluids, showing a shear-thinning behavior, that is, oil viscosity decreases as the shear increases. Mortazavi-Manesh and Shaw [21,34], Bazyleva et al. [62], Mozaffari et al. [87], Tao and Xu [88], and Taborda et al. [44] found similar results. Clearly, viscosity reductions are detected when adding up to a concentration of 700 mg/L of the material, obtaining the largest viscosity change at 500 mg/L. However, a shear-thinning effect of EHO is visible (viscosity dependent on the shear rate), which is expected behavior in a non-Newtonian fluid. These phenomena (viscosity reduction) are due to the interaction between CFNS and aggregates of asphaltene in the EHO structure. The asphaltene adsorption over the CFNS promotes a breakdown of the viscoelastic network that favors the reduction of their viscosity. The explanation for this phenomenon is widely explained in previous works [38,43–46,89–91].

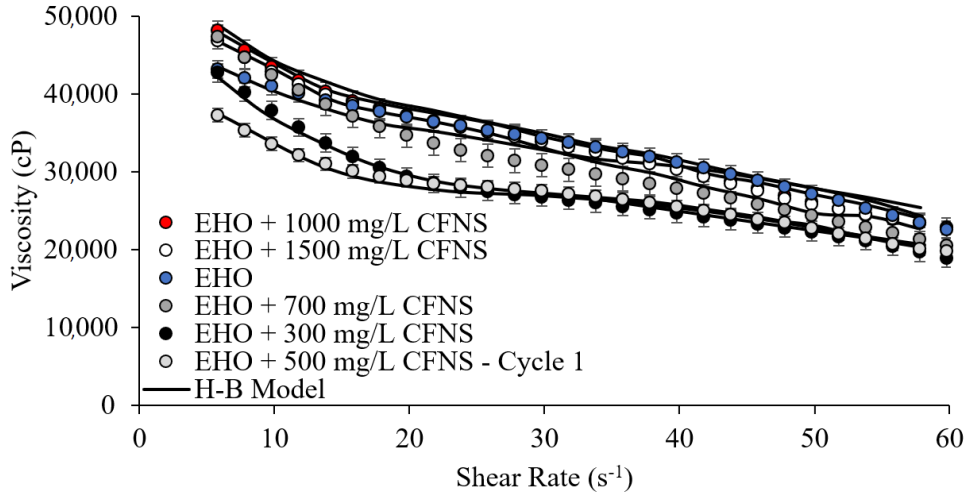

Figure 3. Flow curve for the extra-heavy oils (EHO) on the presence of CFNS at different dosages, and the Herschel–Bulkley model correlation, at 25 °C.

As can be seen in Figure 3, when the concentration exceeds 1000 mg/L, the effect on viscosity reduction is negligible, and a slight increase in viscosity may appear in the mixture of EHO and CFNS. This is due to an agglomeration effect of the nanoparticles themselves inside the highly viscous fluid. The agglomeration causes the particles to behave as larger solids, reducing the interaction with asphaltenes and promoting an increase in viscosity, according to Einstein's theory of viscosity [92]. Figure 4 shows the degree of viscosity reduction for all CFNS dosages evaluated in EHO, which was performed at low shear rates (7.1 s^{-1}) [93–95]. Notably, at 500 mg/L, a viscosity reduction of 18% was obtained, showing the best performance of CFNS over a wide range of concentrations evaluated. This is a promising result in the search for a nanofluid design capable of enhancing transport processes. Moreover, the process may eventually generate a reduction in the consumption of diluents with economic and energy savings.

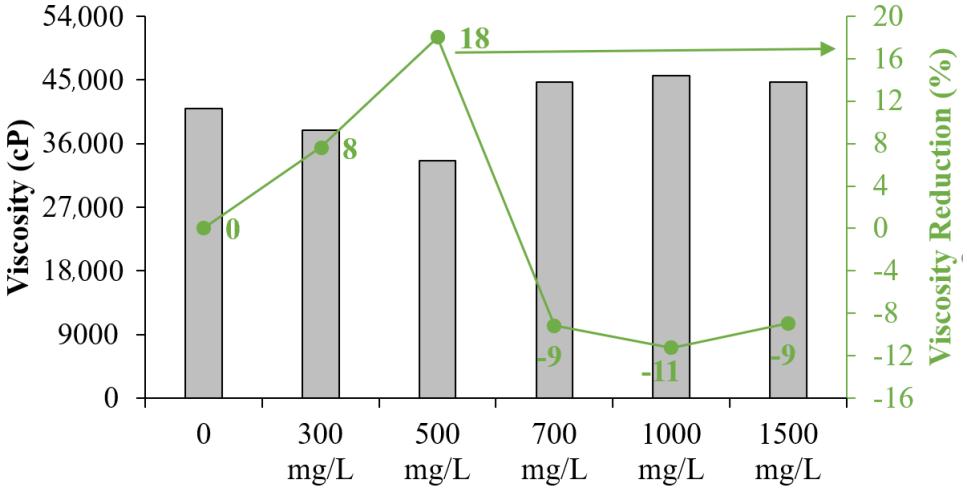

Figure 4. Degree of viscosity reduction for EHO on the presence of CFNS at different dosages, at 25 °C.

For comparison, our previous results indicated the best concentration obtained for the use of nanoparticles in EHO was 1000 mg/L, mainly for SiO_2 nanoparticles.

4.3.2. Second CFNS Cycle for Viscosity Evaluation

Evaluation of the second cycle of CFNS performance was performed by reusing the particles after the first cycle of viscosity reduction. For this process, it was decided to use the dosage that showed the best performance in the first cycle, that is, 500 mg/L. Figure 5 shows the performance of the CFNS in its second cycle of use. It can be seen how the reduction of viscosity is statistically equal to that obtained in the first cycle, which shows the reuse capacity of the particles for reducing EHO viscosity. Note that the performance of the CFNS for the two cycles evaluated showed a similar behavior over the shear rate evaluated. There is a slight deviation between the two measurements, mostly at a shear rate lower than 10 s^{-1}.

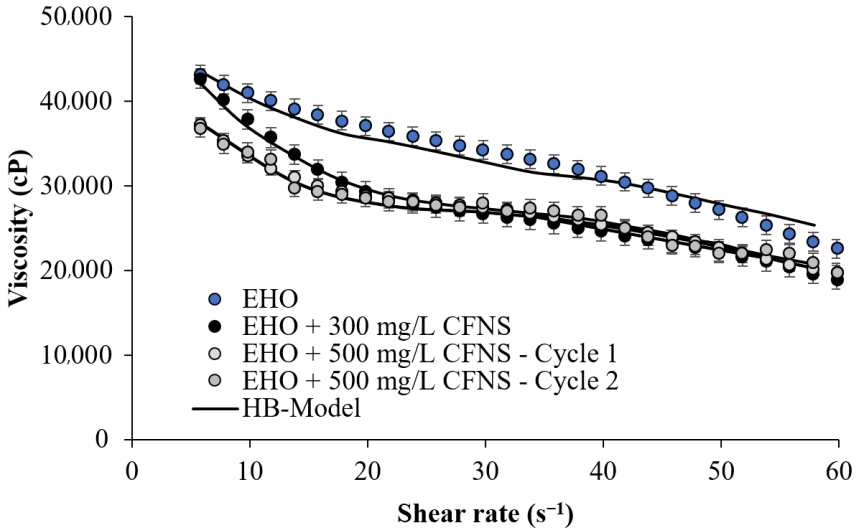

Figure 5. Flow curve for EHO in the presence of CFNS. Comparison of the two evaluated cycles of CFNS use, and the Herschel–Bulkley model correlation at 25 °C.

Notably, nanoparticles have magnetic and adsorptive characteristics that can change over time, so it is necessary in future work to evaluate different operating conditions, for example, testing more than two cycles, evaluating the system at different temperatures, and even changing the type of fluid.

Table 3 shows the H-B parameters for EHO samples with CFNS evaluated. It is seen that $\mu_{\infty,\gamma}$ and K_H decreased as the viscosity decreases, that is, for the addition of CFNS at dosages up to 700 mg/L. Meanwhile, n_H approximates to 1.0 as the amount of CFNS is increased up to 500 mg/L, indicating that the sample tends to be more Newtonian. This result is in agreement with the reported by Mortazavi-Manesh and Shaw [34].

Table 3. Herschel–Bulkley model parameters for mixtures between EHO and different nanoparticles at 25 °C.

Sample	Dosage (mg/L)	H-B Model Parameters				
		K_H (Pa S^n)	n_H	$\mu_{\infty,\gamma}$ (cP)	R^2	*RSME%*
EHO	–	385,700	0.925	6552	0.92	9.2
CFNS cycle 1	300	205,010	0.965	6250	0.91	9.4
	500	102,555	0.975	5450	0.91	9.3
	700	365,850	0.94	6415	0.95	9.9
	1000	405,240	0.921	7355	0.93	9.9
	1500	412,500	0.910	7913	0.94	9.7
CFNS cycle 2	500	105,000	0.975	5578	0.92	9.1
SiO_2	500	98,950	0.981	5365	0.92	9.4

4.3.3. Comparison with SiO_2 Nanoparticles

Figure 6 presents the experimental comparison of the viscosity reduction capacity between the SiO_2 nanoparticles and CFNS. SiO_2 particles are taken as a reference point as previous publications demonstrated it had the best performance in reducing heavy crude oil viscosity [44–46]. Although this figure shows an evaluated concentration of 500 mg/L, the best concentration for this type of nanoparticle has been reported at 1000 mg/L [43,44,46].

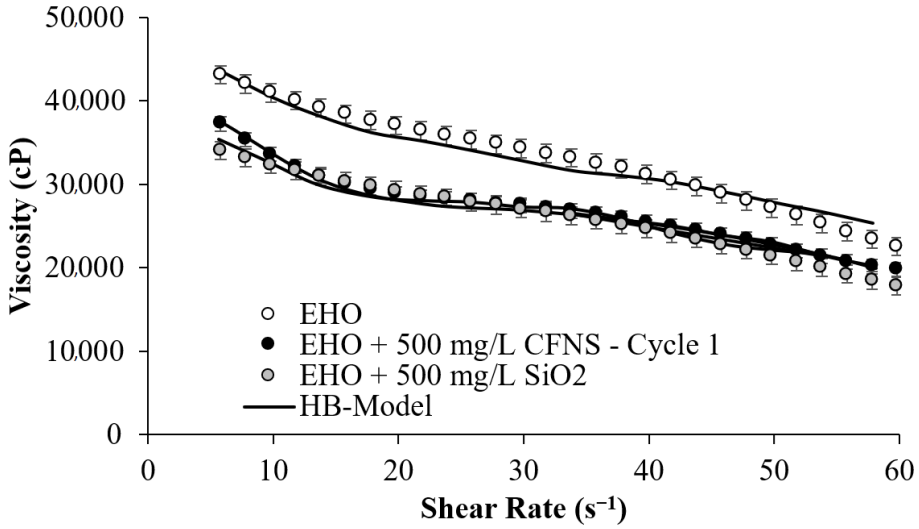

Figure 6. Flow curve for EHO in the presence of CFNS and SiO_2 nanoparticles, and the Herschel–Bulkley model correlation at 25 °C and 500 mg/L.

However, our evaluations have been conducted at the same concentration with the same EHO to observe the rheology behavior for this research. Thus, in Figure 6, both particles produce viscosity reductions, as expected. However, the SiO_2 nanoparticles indicate the same performance, producing a similar change in viscosity for the concentration evaluated. Note SiO_2 nanoparticles at 500 mg/L showed a significant reduction in the same amounts as CFNS. However, it is impossible to reuse SiO_2 nanoparticles due to the difficulty of recovering them from the oil matrix. Hence, the CFNS sample showed promise for being applied in the O&G industry, reducing costs in the dilution process for the transport of EHO.

This finding can be understood from Figure 7, which shows the results quantitatively. The figure shows that the reduction in viscosity of the SiO_2 particles is 22%, slightly higher than the 18% produced by CFNS (evaluated at 7.1 s^{-1}). However, the added value of using CFNS particles lies in the reuse they can have, which considerably reduces the consumption of new material. This can positively impact the economic aspect of the process, which is reflected due to the low consumption of CFNS and diluents compared with conventional methods.

4.4. Dynamic Oscillometry Test

4.4.1. Linear Viscoelasticity Region

Evaluating the viscoelastic moduli alteration is of primary importance to determine how the CFNS leads to changes in the EHO internal structure. At low deformations, the EHO shows a linear trend between stress and strain (linear viscoelastic region), which indicates that the internal structure has not been modified [96]. In general, determining the linear viscoelastic region (LVR) of a material is a relatively simple task, using dynamic rheology tests with amplitude sweeps at a given frequency. Figure 8 shows the amplitude sweep test for EHO with and without 500 mg/L CFNS.

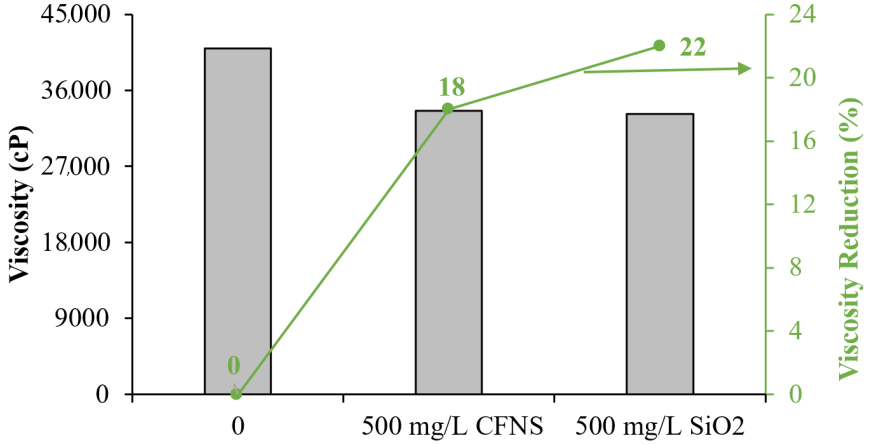

Figure 7. Degree of viscosity reduction for EHO in the presence of CFNS and SiO_2 at 25 °C and 500 mg/L.

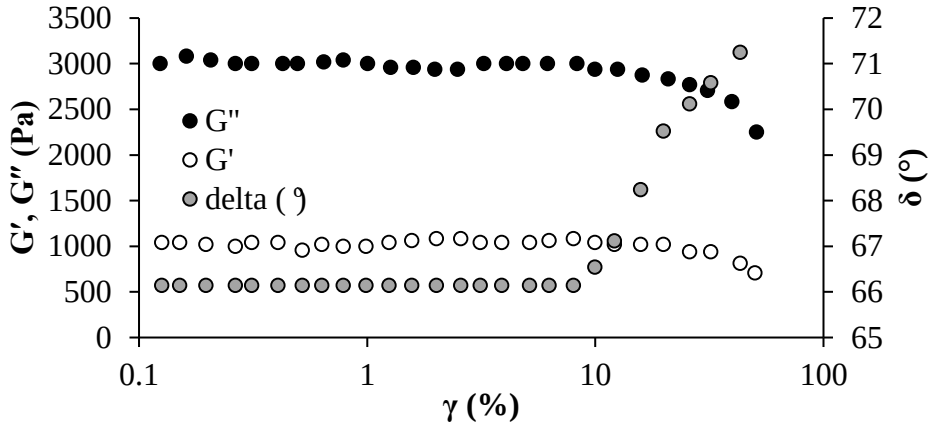

(**a**)

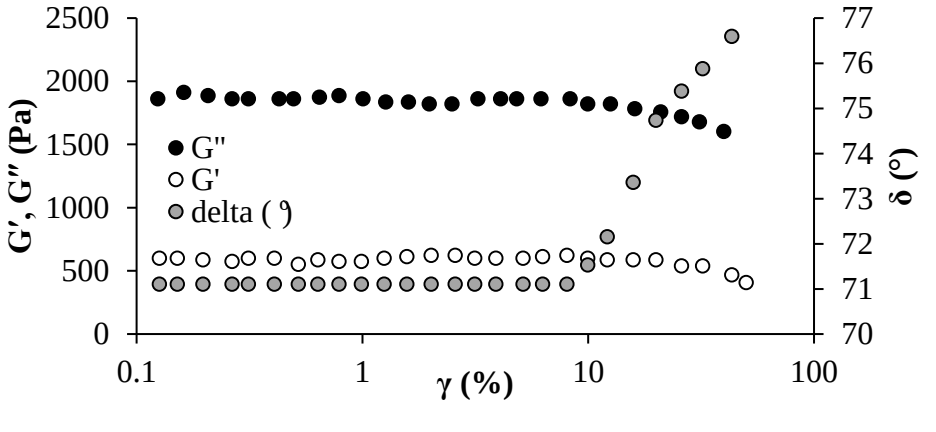

(**b**)

Figure 8. Amplitude sweep test for heavy oil in (**a**) absence and (**b**) presence of 500 mg/L of CFNS at a fixed frequency of 10 rad/s and a temperature of 25 °C.

Figure 8 shows the obtained storage modulus (G′), loss modulus (G′′), and the phase angle (δ). For both EHO in the presence and absence of CFNS, it is observed that as the strain increases up to 2%, the moduli do not change. Hence, the LVR is given for strain values between 0.1 and 10%. G′′ is always higher than G′, indicating that the sample's

behavior is more viscous than elastic. The G′ decreases when 500 mg/L of CFNS are added to the EHO, suggesting lower internal resistance and lower viscosity. Meanwhile, δ is always higher than 45°, indicating a liquid-like behavior [96–98].

From Figure 8, it is observed that the LVR is slightly higher upon CFNS addition, indicating an internal structure change in the EHO [61]. Further, the frequency analysis is carried out in the LVR to determine the effect of CFNS on the EHO viscoelastic properties.

4.4.2. Frequency Sweep Test for Heavy Crude Oil

For angular frequency analysis, deformation was fixed at 2%, and the sweep was carried out at 25 °C between 0.1 to 100 rad/s. Figure 9 shows G′, G″, and δ at 25 °C in the absence and presence of CFNS. From Figure 9, it is observed that in the absence of the nanomaterial, G″ is higher than G′, indicating a more viscous behavior than an elastic one. The moduli also increase as the angular frequency increases, attributed to the asphaltene distribution in the EHO matrix and the viscoelastic network formation due to strong colloidal forces [63,99–101].

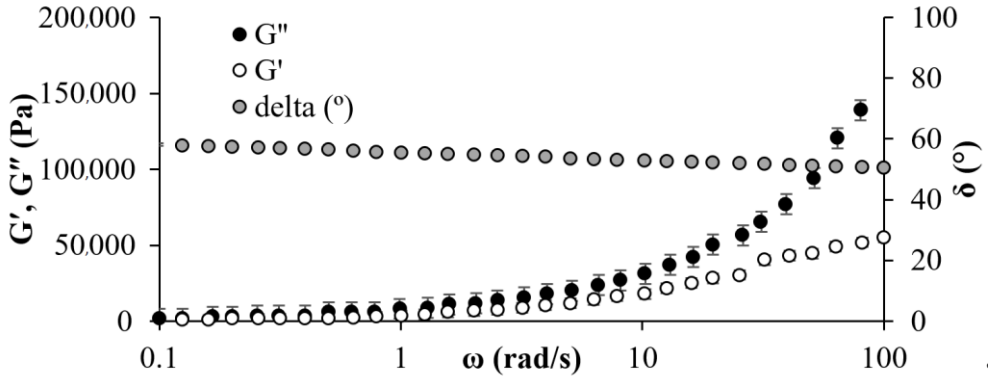

(**a**)

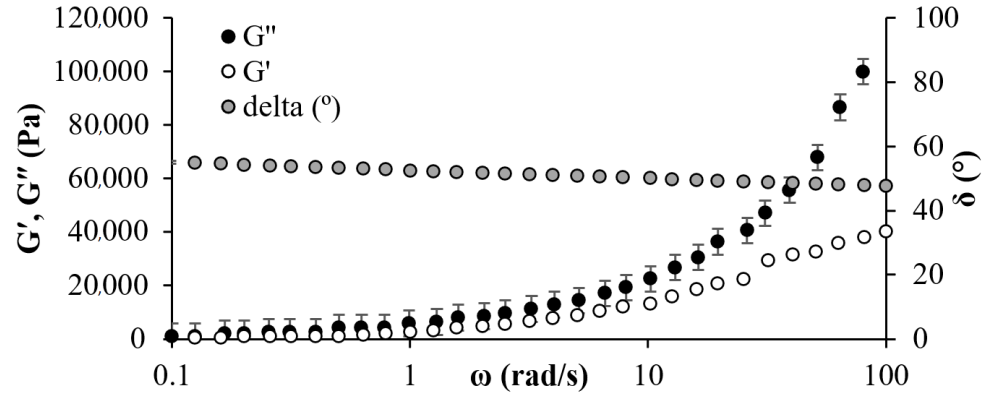

(**b**)

Figure 9. Master curve for heavy oil in (**a**) absence and (**b**) presence of 500 mg/L of CFNS at 25 °C and a fixed strain of 2%.

In the case of the EHO in the presence of CFNS, the G″ is also greater than G′. Nevertheless, the moduli decreased by approximately 30% regarding the system without nanoparticles, corroborating the decrease of dynamic viscosity due to the decrease in viscous and elastic contributions. This viscosity reduction upon CFNS addition would positively impact the optimization of operating conditions related to the production, recovery and transport of EHO.

5. Conclusions

CFNS is composed of nanospheric particles (150 nm) containing three phases: cubic-$CuFe_2O_4$ (67.5%), Cu_2O (17.1%), and Cu (15.4%). XPS showed that Fe^{3+} was placed in A and B sites and the presence of metallic Cu and Cu^+ ions. CFNS had a high M_S value and very low M_R/M_S ratios, indicating substantial superparamagnetic behavior. The rheological evaluation carried out reflects a viscosity reduction of up to 18% by adding 500 mg/L of CFNS. The rheological curve described by the extra-heavy crude oil sample in the presence and absence of CFNS defines a shear-thinning-type pseudoplastic behavior, typical of this class of fluids, where the viscosity decreases as the shear rate increases. The nanoparticles were evaluated in their optimal concentration in two cycles, representing the use and reuse of the magnetic particles. We identify significant decreases in the elastic and viscous moduli through dynamic rheology tests, causing internal changes in the viscoelastic modules, which are responsible for a reduction in the viscosity of the crude oil. The adsorption isotherms constructed demonstrate an existing interaction between asphaltenes from heavy crude oil and CFNS. The main characteristic of CFNS-type materials is their high magnetic power and their ability to reduce the viscosity of heavy crude oils. Both properties offer advantages to the chemical addition processes to enhance the transport and mobility processes of heavy crude oils, allowing the reuse of nanoparticles and the reduction of diluents. This could generate technological, economic and environmental impacts for the oil and gas industry.

Author Contributions: Conceptualization, all authors; methodology, L.M. and E.A.T.; formal analysis, all authors; investigation, L.M. and E.A.T.; data curation, C.M.-C. and F.B.C.; writing—original draft preparation, L.M. and E.A.T.; writing—review and editing, all authors; visualization, F.B.C. All authors have read and agreed to the published version of the manuscript.

Funding: C.M.-C acknowledges financial support from the Spanish Project ref. RTI2018-099,224-B-I00 from ERDF/Ministry of Science, Innovation and Universities—State Research Agency. M.V.L.-R. acknowledges financial support from Junta de Andalucía, Spain, RNM-366 research group.

Data Availability Statement: The data presented in this study are available on request from the corresponding author.

Acknowledgments: L.M. thanks the Asociación Universitaria Iberoamericana de Postgrado (AUIP) and University of Jaén for supporting her PhD studies. The authors from Grupo de Investigación Fenómenos de Superficie Michael Polanyi acknowledge Universidad Nacional de Colombia for the financial and logistical support. Special thanks to Eng. Daniel Montes.

Conflicts of Interest: The authors declare no conflict of interest.

References

1. Hirsch, R.L.; Bezdek, R.; Wendling, R. Peaking of world oil production and its mitigation. *AIChE J.* **2005**, *52*, 2–8. [CrossRef]
2. Williams, B. Heavy hydrocarbons playing key role in peak-oil debate, future energy supply. *Oil Gas J.* **2003**, *101*, 20–27.
3. Bera, A.; Babadagli, T. Status of electromagnetic heating for enhanced heavy oil/bitumen recovery and future prospects: A review. *Appl. Energy* **2015**, *151*, 206–226. [CrossRef]
4. Franco, C.; Flórez, A.; Ochoa, M. Análisis de la cadena de suministros de biocombustibles en Colombia. *Rev. Dinámica Sist.* **2008**, *4*, 109–133.
5. Adams, J. Asphaltene adsorption, a literature review. *Energy Fuels* **2014**, *28*, 2831–2856. [CrossRef]
6. Chavan, S.; Kini, H.; Ghosal, R. Process for sulfur reduction from high viscosity petroleum oils. *Int. J. Environ. Sci. Dev.* **2012**, *3*, 228–231. [CrossRef]
7. Chew, K.J. The future of oil: Unconventional fossil fuels. *Philos. Trans. R. Soc. A Math. Phys. Eng. Sci.* **2014**, *372*, 20120324. [CrossRef]
8. Ghanavati, M.; Shojaei, M.-J.; Saadatabadi, A.R. Effects of asphaltene content and temperature on viscosity of Iranian heavy crude oil: Experimental and modeling study. *Energy Fuels* **2013**, *27*, 7217–7232. [CrossRef]
9. Groenzin, H.; Mullins, O.C. Asphaltene molecular size and structure. *J. Phys. Chem. A* **1999**, *103*, 11237–11245. [CrossRef]
10. Hinkle, A.; Shin, E.-J.; Liberatore, M.W.; Herring, A.M.; Batzle, M. Correlating the chemical and physical properties of a set of heavy oils from around the world. *Fuel* **2008**, *87*, 3065–3070. [CrossRef]
11. Khalil, M.; Jan, B.M.; Tong, C.W.; Berawi, M.A. Advanced nanomaterials in oil and gas industry: Design, application and challenges. *Appl. Energy* **2017**, *191*, 287–310. [CrossRef]

12. Meyer, R.F.; Attanasi, E. *Heavy Oil and Natural Bitumen : Strategic Petroleum Resources*; US Geological Survey: Reston, VA, USA, 2003; Volume 434, pp. 650–657.
13. Al-Maamari, R.S.; Buckley, J.S. Asphaltene precipitation and alteration of wetting: The potential for wettability changes during oil production. *SPE Reserv. Eval. Eng.* **2003**, *6*, 210–214. [CrossRef]
14. Gharfeh, S.; Yen, A.; Asomaning, S.; Blumer, D. Asphaltene flocculation onset determinations for heavy crude oil and its implications. *Pet. Sci. Technol.* **2004**, *22*, 1055–1072. [CrossRef]
15. Kojima, T.; Tahara, K. Refinement and transportation of petroleum with hydrogen from renewable energy. *Energy Convers. Manag.* **2001**, *42*, 1839–1851. [CrossRef]
16. Oskui, G.; Jumaa, M.; Folad, E.G.; Rashed, A. Systematic approach for prevention and remediation of asphaltene problems during CO_2/hydrocarbon injection project. In Proceedings of the Twenty-First International Offshore and Polar Engineering Conference, Maui, Hawaii, USA, 19–24 June 2011; International Society of Offshore and Polar Engineers: Cupertino, CA, USA, 2011.
17. Alvarez, G.; Poteau, S.; Argillier, J.-F.; Langevin, M.; Salager, J.-L. Heavy oil−water interfacial properties and emulsion stability: Influence of dilution. *Energy Fuels* **2009**, *23*, 294–299. [CrossRef]
18. Gutierrez, J.G. Plan de Inversiones ECOPETROL. 2011, p. 34. Available online: www.infraestructura.org.co (accessed on 6 January 2021).
19. Hasan, S.W.; Ghannam, M.T.; Esmail, N. Heavy crude oil viscosity reduction and rheology for pipeline transportation. *Fuel* **2010**, *89*, 1095–1100. [CrossRef]
20. López, E.; Montes, E.; Garavito, A.; Collazos, M.M. La economía petrolera en Colombia (Parte II). Relaciones intersectoriales e importancia en la economía nacional. *Borradores Econ.* **2013**, *748*, 1–58.
21. Mortazavi-Manesh, S.; Shaw, J.M. Thixotropic rheological behavior of maya crude oil. *Energy Fuels* **2014**, *28*, 972–979. [CrossRef]
22. Al-Roomi, Y.; George, R.; Elgibaly, A.; Elkamel, A. Use of a novel surfactant for improving the transportability/transportation of heavy/viscous crude oils. *J. Pet. Sci. Eng.* **2004**, *42*, 235–243. [CrossRef]
23. Bensakhria, A.; Peysson, Y.; Antonini, G. Experimental study of the pipeline lubrication for heavy oil transport. *Oil Gas. Sci. Technol. Rev. de l'IFP* **2004**, *59*, 523–533. [CrossRef]
24. Chang, C.; Nguyen, Q.; Rønningsen, H.P. Isothermal start-up of pipeline transporting waxy crude oil. *J. Non-Newton. Fluid Mech.* **1999**, *87*, 127–154. [CrossRef]
25. Gateau, P.; Henaut, I.; Barré, L.; Argillier, J.F. Heavy oil dilution. *Oil Gas. Sci. Technol. Rev. de l'IFP* **2004**, *59*, 503–509. [CrossRef]
26. Isaac, J.D.; Speed, J.B. Method of Piping Fluids. U.S. Patent 759,374A, 1 May 1904.
27. Joseph, D.D.; Bai, R.; Chen, K.P.; Renardy, Y.Y. Core-annular flows. *Annu. Rev. Fluid Mech.* **1997**, *29*, 65–90. [CrossRef]
28. Kessick, M.A.; Denis, C.E.S. Pipeline Transportation of Heavy Crude Oil. U.S. Patent 4343323, 12 August 1982.
29. Khan, M.R. Rheological properties of heavy oils and heavy oil emulsions. *Energy Sources* **1996**, *18*, 385–391. [CrossRef]
30. McKibben, M.J.; Gillies, R.G.; Shook, C.A. A laboratory investigation of horizontal well heavy oil-water flows. *Can. J. Chem. Eng.* **2000**, *78*, 743–751. [CrossRef]
31. Saniere, A.; Hénaut, I.; Argillier, J.F. Pipeline transportation of heavy oils, a strategic, economic and technological challenge. *Oil Gas. Sci. Technol. Rev. de l'IFP* **2004**, *59*, 455–466. [CrossRef]
32. Selim, M.Y.E. Reducing the viscosity of Jojoba Methyl Ester diesel fuel and effects on diesel engine performance and roughness. *Energy Convers. Manag.* **2009**, *50*, 1781–1788. [CrossRef]
33. Castro, J. Perspectivas de la demanda energética global. *Petrotecnia* **2011**, *February*, 54–70.
34. Mortazavi-Manesh, S.; Shaw, J.M. Effect of diluents on the rheological properties of maya crude oil. *Energy Fuels* **2016**, *30*, 766–772. [CrossRef]
35. Urquhart, R. Heavy oil transportation—Present and future. *J. Can. Pet. Technol.* **1986**, *25*. [CrossRef]
36. Langevin, D.; Argillier, J.-F. Interfacial behavior of asphaltenes. *Adv. Colloid Interface Sci.* **2016**, *233*, 83–93. [CrossRef] [PubMed]
37. Martínez-Palou, R.; Mosqueira, M.D.L.; Zapata-Rendón, B.; Mar-Juárez, E.; Bernal-Huicochea, C.; Clavel-López, J.D.L.C.; Aburto, J. Transportation of heavy and extra-heavy crude oil by pipeline: A review. *J. Pet. Sci. Eng.* **2011**, *75*, 274–282. [CrossRef]
38. Briceno, M.I.; Salager, J.-L.; Bracho, C.L. Heavy Hydrocarbon Emulsions Making Use of the State of the Art in Formulation Engineering. In *Encyclopedic Handbook of Emulsion Technology*; Sjöblom, J., Ed.; Publ. Marcel Dekker: New York, NY, USA, 2001; Volume 20, pp. 455–495.
39. Anto, R.; Deshmukh, S.; Sanyal, S.; Bhui, U.K. Nanoparticles as flow improver of petroleum crudes: Study on temperature-dependent steady-state and dynamic rheological behavior of crude oils. *Fuel* **2020**, *275*, 117873. [CrossRef]
40. Contreras–Mateus, M.D.; López–López, M.T.; Ariza-León, E.; Chaves-Guerrero, A. Rheological implications of the inclusion of ferrofluids and the presence of uniform magnetic field on heavy and extra-heavy crude oils. *Fuel* **2021**, *285*, 119184. [CrossRef]
41. Ke, H.; Yuan, M.; Xia, S. A review of nanomaterials as viscosity reducer for heavy oil. *J. Dispers. Sci. Technol.* **2020**, 1–12. [CrossRef]
42. Sun, Y.; Yang, D.; Shi, L.; Wu, H.; Cao, Y.; He, Y.; Xie, T. Properties of nanofluids and their applications in enhanced oil recovery: A comprehensive review. *Energy Fuels* **2020**, *34*, 1202–1218. [CrossRef]
43. Taborda, E.A.; Alvarado, V.; Cortés, F.B. Effect of SiO 2 -based nanofluids in the reduction of naphtha consumption for heavy and extra-heavy oils transport: Economic impacts on the Colombian market. *Energy Convers. Manag.* **2017**, *148*, 30–42. [CrossRef]
44. Taborda, E.A.; Alvarado, V.; Franco, C.A.; Cortés, F.B. Rheological demonstration of alteration in the heavy crude oil fluid structure upon addition of nanoparticles. *Fuel* **2017**, *189*, 322–333. [CrossRef]

45. Taborda, E.A.; Franco, C.A.; Lopera, S.H.; Alvarado, V.; Cortés, F.B. Effect of nanoparticles/nanofluids on the rheology of heavy crude oil and its mobility on porous media at reservoir conditions. *Fuel* **2016**, *184*, 222–232. [CrossRef]
46. Taborda, E.A.; Franco, C.A.; Ruiz, M.A.; Alvarado, V.; Cortés, F.B. Experimental and theoretical study of viscosity reduction in heavy crude oils by addition of nanoparticles. *Energy Fuels* **2017**, *31*, 1329–1338. [CrossRef]
47. Moreno-Castilla, C.; López-Ramón, M.V.; Fontecha-Cámara, M. Ángeles; Álvarez, M.; Mateus, L. Removal of phenolic compounds from water using copper ferrite nanosphere composites as fenton catalysts. *Nanomaterials* **2019**, *9*, 901. [CrossRef] [PubMed]
48. Fontecha-Camara, M.A.; Moreno-Castilla, C.; López-Ramón, M.V.; Álvarez, M.A. Mixed iron oxides as Fenton catalysts for gallic acid removal from aqueous solutions. *Appl. Catal. B Environ.* **2016**, *196*, 207–215. [CrossRef]
49. Yabuki, A.; Tanaka, S. Oxidation behavior of copper nanoparticles at low temperature. *Mater. Res. Bull.* **2011**, *46*, 2323–2327. [CrossRef]
50. Chen, W.; Fan, Z.; Lai, Z. Synthesis of core-shell heterostructured Cu/Cu2O nanowires monitored by in situ XRD as efficient visible-light photocatalysts. *J. Mater. Chem. A* **2013**, *1*, 13862–13868. [CrossRef]
51. Zhao, W.; Zhang, S.; Ding, J.; Deng, Z.; Guo, L.; Zhong, Q. Enhanced catalytic ozonation for NOx removal with $CuFe_2O_4$ nanoparticles and mechanism analysis. *J. Mol. Catal. A Chem.* **2016**, *424*, 153–161. [CrossRef]
52. Cortés, F.B.; Ruiz, M.A.; Benjumea, P.; Patiño, E.; Franco Ariza, C.A. Kinetic and thermodynamic equilibrium of asphaltenes sorption onto nanoparticles of nickel oxide supported on nanoparticulated alumina. *Fuel* **2013**, *105*, 408–414.
53. Franco, C.A.; Montoya, T.; Nassar, N.N.; Pereira-Almao, P.; Cortés, F.B. Adsorption and subsequent oxidation of colombian asphaltenes onto nickel and/or palladium oxide supported on fumed silica nanoparticles. *Energy Fuels* **2013**, *27*, 7336–7347. [CrossRef]
54. Nassar, N.N.; Hassan, A.; Pereira-Almao, P. Effect of the particle size on asphaltene adsorption and catalytic oxidation onto alumina particles. *Energy Fuels* **2011**, *25*, 3961–3965. [CrossRef]
55. Nassar, N.N. Asphaltene adsorption onto alumina nanoparticles: Kinetics and thermodynamic studies. *Energy Fuels* **2010**, *24*, 4116–4122. [CrossRef]
56. Franco, C.A.; Lozano, M.M.; Acevedo, S.; Nassar, N.N.; Cortés, F.B. Effects of resin I on asphaltene adsorption onto nanoparticles: A novel method for obtaining asphaltenes/resin isotherms. *Energy Fuels* **2016**, *30*, 264–272. [CrossRef]
57. Nassar, N.N.; Franco, C.A.; Montoya, T.; Cortés, F.B.; Hassan, A. Effect of oxide support on Ni–Pd bimetallic nanocatalysts for steam gasification of n-C 7 asphaltenes. *Fuel* **2015**, *156*, 110–120. [CrossRef]
58. Cortés, F.B.; Montoya, T.; Acevedo, S.; Nassar, N.N.; Franco, C.A. Adsorption-desorption of n–C7 asphaltenes over micro- and nanoparticles of silica and its impact on wettability alteration. *CTF—Ciencia Tecnología Futuro* **2016**, *6*, 89–106. [CrossRef]
59. Guzmán, J.D.; Betancur, S.; Carrasco-Marín, F.; Franco, C.A.; Nassar, N.N.; Cortés, F.B. Importance of the adsorption method used for obtaining the nanoparticle dosage for asphaltene-related treatments. *Energy Fuels* **2015**, *30*, 2052–2059. [CrossRef]
60. Chen, D.T.N.; Wen, Q.; Janmey, P.A.; Crocker, J.C.; Yodh, A.G. Rheology of soft materials. *Annu. Rev. Condens. Matter Phys.* **2010**, *1*, 301–322. [CrossRef]
61. Visintin, R.F.G.; Lapasin, R.; Vignati, E.; D'Antona, P.; Lockhart, T.P. Rheological behavior and structural interpretation of waxy crude oil gels. *Langmuir* **2005**, *21*, 6240–6249. [CrossRef]
62. Bazyleva, A.B.; Hasan, A.; Fulem, M.; Becerra, M.; Shaw, J.M. Bitumen and heavy oil rheological properties: Reconciliation with viscosity measurements. *J. Chem. Eng. Data* **2010**, *55*, 1389–1397. [CrossRef]
63. Behzadfar, E.; Hatzikiriakos, S.G. Viscoelastic properties and constitutive modelling of bitumen. *Fuel* **2013**, *108*, 391–399. [CrossRef]
64. Dimitriou, C.J.; McKinley, G.H. A comprehensive constitutive law for waxy crude oil: A thixotropic yield stress fluid. *Soft Matter* **2014**, *10*, 6619–6644. [CrossRef]
65. Ershov, D.; Stuart, M.C.; Van Der Gucht, J. Mechanical properties of reconstituted actin networks at an oil-water interface determined by microrheology. *Soft Matter* **2012**, *8*, 5896. [CrossRef]
66. Montoya, T.; Coral, D.; Franco, C.A.; Nassar, N.N.; Cortés, F.B. A novel solid-liquid equilibrium model for describing the adsorption of associating asphaltene molecules onto solid surfaces based on the "Chemical Theory". *Energy Fuels* **2014**, *28*, 4963–4975. [CrossRef]
67. Talu, O.; Meunier, F. Adsorption of associating molecules in micropores and application to water on carbon. *AIChE J.* **1996**, *42*, 809–819. [CrossRef]
68. Buckley, S.; Leverett, M. Mechanism of fluid displacement in sands. *Trans. AIME* **1942**, *146*, 107–116. [CrossRef]
69. Herschel, W.H. The Change in viscosity of oils with the temperature. *J. Ind. Eng. Chem.* **1922**, *14*, 715–722. [CrossRef]
70. Preece, D.A.; Montgomery, D.C. Design and analysis of experiments. *Int. Stat. Rev.* **1978**, *46*, 120. [CrossRef]
71. Nassar, N.N.; Betancur, S.; Acevedo, S.; Franco, C.A.; Cortés, F.B. Development of a population balance model to describe the influence of shear and nanoparticles on the aggregation and fragmentation of asphaltene aggregates. *Ind. Eng. Chem. Res.* **2015**, *54*, 8201–8211. [CrossRef]
72. Nik, W.W.; Ani, F.N.; Masjuki, H.; Giap, S.E. Rheology of bio-edible oils according to several rheological models and its potential as hydraulic fluid. *Ind. Crop. Prod.* **2005**, *22*, 249–255. [CrossRef]
73. Sarpkaya, T. Flow of non-Newtonian fluids in a magnetic field. *AIChE J.* **1961**, *7*, 324–328. [CrossRef]
74. Shao, S.; Lo, E.Y. Incompressible SPH method for simulating Newtonian and non-Newtonian flows with a free surface. *Adv. Water Resour.* **2003**, *26*, 787–800. [CrossRef]

75. Ding, Y.; Zhu, L.; Wang, N.; Tang, H. Sulfate radicals induced degradation of tetrabromobisphenol A with nanoscaled magnetic CuFe2O4 as a heterogeneous catalyst of peroxymonosulfate. *Appl. Catal. B Environ.* **2013**, *129*, 153–162. [CrossRef]
76. Erdoğan, İ.Y.; Güllü, Ö. Optical and structural properties of CuO nanofilm: Its diode application. *J. Alloy. Compd.* **2010**, *492*, 378–383. [CrossRef]
77. Selvan, R.; Augustin, C.; Berchmans, L.; Saraswathi, R. Combustion synthesis of $CuFe_2O$. *Mater. Res. Bull.* **2003**, *38*, 41–54. [CrossRef]
78. Silva, M.; Silva, F.; Sinfrônio, F.S.M.; Paschoal, A.; Silva, E.; Paschoal, C. The effect of cobalt substitution in crystal structure and vibrational modes of CuFe2O4 powders obtained by polymeric precursor method. *J. Alloy. Compd.* **2014**, *584*, 573–580. [CrossRef]
79. Waldron, R.D. Infrared spectra of ferrites. *Phys. Rev.* **1955**, *99*, 1727–1735. [CrossRef]
80. Wu, F.; Li, X.; Wang, Z.; Xu, C.; He, H.; Qi, A.; Yin, X.; Guo, H. Preparation of high-value TiO_2 nanowires by leaching of hydrolyzed titania residue from natural ilmenite. *Hydrometallurgy* **2013**, *140*, 82–88. [CrossRef]
81. Xiong, Z.; Cao, J.; Lai, B.; Yang, P. Comparative study on degradation of p -nitrophenol in aqueous solution by $mFe/Cu/O_3$ and mFe_0/O_3 processes. *J. Ind. Eng. Chem.* **2018**, *59*, 196–207. [CrossRef]
82. He, Z.; Song, S.; Ying, H.; Xu, L.; Chen, J. p-Aminophenol degradation by ozonation combined with sonolysis: Operating conditions influence and mechanism. *Ultrason. Sonochem.* **2007**, *14*, 568–574. [CrossRef]
83. Sun, M.; Yao, R.; You, Y.; Deng, S.; Gao, W. Degradation of 4-aminophenol by hydrogen peroxide oxidation using enzyme from Serratia marcescens as catalyst. *Front. Environ. Sci. Eng. China* **2007**, *1*, 95–98. [CrossRef]
84. Calemma, V.; Iwanski, P.; Nali, M.; Scotti, R.; Montanari, L. Structural characterization of asphaltenes of different origins. *Energy Fuels* **1995**, *9*, 225–230. [CrossRef]
85. Arias-Madrid, D.; Medina, O.E.; Gallego, J.; Acevedo, S.; Correa-Espinal, A.A.; Cortés, F.B.; Franco, C.A. NiO, Fe_2O_3, and MoO_3 supported over SiO_2 nanocatalysts for asphaltene adsorption and catalytic decomposition: Optimization through a simplex-centroid mixture design of experiments. *Catalysts* **2020**, *10*, 569. [CrossRef]
86. Ascanius, B.E.; Garcia, D.M.; Andersen, S.I. Analysis of asphaltenes subfractionated byN-Methyl-2-pyrrolidone. *Energy Fuels* **2004**, *18*, 1827–1831. [CrossRef]
87. Mozaffari, S.; Tchoukov, P.; Atias, J.; Czarnecki, J.; Nazemifard, N. Effect of asphaltene aggregation on rheological properties of diluted athabasca bitumen. *Energy Fuels* **2015**, *29*, 5595–5599. [CrossRef]
88. Tao, R.; Xu, X. Reducing the viscosity of crude oil by pulsed electric or magnetic field. *Energy Fuels* **2006**, *20*, 2046–2051. [CrossRef]
89. Andreatta, G.; Bostrom, N.; Mullins, O.C. High-Q ultrasonic determination of the critical nanoaggregate concentration of asphaltenes and the critical micelle concentration of standard surfactants. *Langmuir* **2005**, *21*, 2728–2736. [CrossRef] [PubMed]
90. Andreatta, G.; Bostrom, N.; Mullins, O.C. Ultrasonic spectroscopy of asphaltene aggregation. In *Asphaltenes, Heavy Oils, and Petroleomics*; Springer Science and Business Media LLC: Berlin/Heidelberg, Germany, 2007; pp. 231–257.
91. Yang, X.; Czarnecki, J. Tracing sodium naphthenate in asphaltenes precipitated from athabasca bitumen. *Energy Fuels* **2005**, *19*, 2455–2459. [CrossRef]
92. Einstein, A. Eine neue bestimmung der moleküldimensionen. *Ann. Phys.* **1906**, *324*, 289–306. [CrossRef]
93. Maya, G.A.; Sierra, D.P.M.; Castro, R.H.; Portillo, M.L.T.; Soto, C.P.; Perez, H.H. Enhanced oil recovery (EOR) status—Colombia. In Proceedings of the Latin American & Caribbean Petroleum Engineering Conference, Lima, Peru, 1–3 December 2010.
94. García, R.H.C.; Toro, G.A.M.; Diaz, R.J.; Perez, H.I.Q.; Guardia, V.M.D.; Vargas, K.M.C.; Bustamante, J.M.P.; Aya, C.L.D.; Romero, R.A.P. Polymer flooding to improve volumetric sweep efficiency in waterflooding processes. *CTF—Ciencia Tecnología Futuro* **2016**, *6*, 71–90. [CrossRef]
95. Giraldo, L.J.; Giraldo, M.A.; Gallo, S.L.; Maya, G.; Zabala, R.D.; Nassar, N.N.; Franco, C.A.; Alvarado, V.; Cortés, F.B. The effects of SiO2 nanoparticles on the thermal stability and rheological behavior of hydrolyzed polyacrylamide based polymeric solutions. *J. Pet. Sci. Eng.* **2017**, *159*, 841–852. [CrossRef]
96. Ghannam, M.T.; Hasan, S.W.; Abu-Jdayil, B.; Esmail, N. Rheological properties of heavy & light crude oil mixtures for improving flowability. *J. Pet. Sci. Eng.* **2012**, *81*, 122–128. [CrossRef]
97. Behura, J.; Batzle, M.; Hofmann, R.; Dorgan, J. Heavy oils: Their shear story. *Geophysics* **2007**, *72*, E175–E183. [CrossRef]
98. Lesueur, D. The colloidal structure of bitumen: Consequences on the rheology and on the mechanisms of bitumen modification. *Adv. Colloid Interface Sci.* **2009**, *145*, 42–82. [CrossRef]
99. Mullins, O.C.; Betancourt, S.S.; Cribbs, M.E.; Dubost, F.X.; Creek, J.L.; Andrews, A.B.; Venkataramanan, L. The colloidal structure of crude oil and the structure of oil reservoirs. *Energy Fuels* **2007**, *21*, 2785–2794. [CrossRef]
100. Wong, G.K.; Yen, T.F. An electron spin resonance probe method for the understanding of petroleum asphaltene macrostructure. *J. Pet. Sci. Eng.* **2000**, *28*, 55–64. [CrossRef]
101. Yen, T.F.; Chilingarian, G.V. *Asphaltenes and Asphalts*, 1st ed.; Elsevier: Amsterdam, The Netherlands, 2000.